

## The 762 nm emissions of sprites

C. L. Kuo,<sup>1,2</sup> S. C. Chang,<sup>1</sup> L. J. Lee,<sup>1</sup> T. Y. Huang,<sup>1,3</sup> A. B. Chen,<sup>4</sup> H. T. Su,<sup>1,2</sup>  
R. R. Hsu,<sup>1,2</sup> D. D. Sentman,<sup>5</sup> H. U. Frey,<sup>6</sup> S. B. Mende,<sup>6</sup> Y. Takahashi,<sup>7</sup> and L. C. Lee<sup>8</sup>

Received 19 July 2010; revised 1 November 2010; accepted 3 November 2010; published 22 January 2011.

[1] We report the 762 nm emissions in sprites recorded by the ISUAL experiment onboard the FORMOSAT-2 satellite. The 762 nm imager filter is centered at 763.3 nm with a 7 nm bandwidth at 50% transmittance. Sprite emissions in this passband include the N<sub>2</sub> first positive (1PN<sub>2</sub>) bands, (2, 0) and (3, 1), the O<sub>2</sub> atmospheric (atm) band (0, 0), and the hydroxyl (4, 0) emissions. Because these mixed emissions cannot be resolved in the 762 nm narrowband filter, a zero-dimensional plasma chemistry model is used to estimate the expected relative intensities of these emission bands in sprites. The computed 1PN<sub>2</sub> brightness in a single streamer is 1.4 MR and 2.6 kR for the O<sub>2</sub> atm band emissions at frame integration times of 30 ms. In the 762 nm passband, the 1PN<sub>2</sub> emissions are the dominant emissions in sprites, and the ratio of 1PN<sub>2</sub> to O<sub>2</sub> atmospheric emissions is ~500, while the hydroxyl emissions can be neglected. In this ISUAL 762 nm campaign, the brightest sprite out of the four recorded events has possible O<sub>2</sub> atm band emissions that lasted more than 90 ms, and its observed brightness is consistent with the model prediction. Even though the lightning 762 nm emissions are strongly absorbed by O<sub>2</sub> below 60 km, the ISUAL observed parent lightning emissions in this passband are still more than a factor of two brighter than those from ISUAL observed sprites. Hence for spacecraft nadir TLE detection missions, 762 nm bands may not be used as the sole signature to identify sprites, and auxiliary emission bands are needed.

**Citation:** Kuo, C. L., et al. (2011), The 762 nm emissions of sprites, *J. Geophys. Res.*, *116*, A01310, doi:10.1029/2010JA015949.

### 1. Introduction

[2] A sprite is one of several types of transient luminous events (TLEs) induced in the upper atmosphere by thunderstorms, and it usually occurs in the altitude range of 40–90 km [Sentman et al., 1995]. Telescopic images of sprites show the existence of narrow filamentary plasma structures in sprites, called streamers. The radius of sprite streamers is tens to hundreds of meters at sprite altitudes of ~70 km [Gerken et al., 2000; Gerken and Inan, 2003]. The measured streamer radius is consistent with predictions from numerical simulation of streamers [Pasko et al., 1998]. A streamer can

initiate from a single electron avalanche at sprite altitudes and develop into a propagating ionization wave driven by a weak background electric field [Liu and Pasko, 2004, and references therein]. The inferred electric field derived from spectroscopic analysis [Kuo et al., 2005] or streamer modeling [Liu and Pasko, 2005; Liu et al., 2006] indicates a high electric field in the streamer head, which can trigger a series of chemical reactions. Sentman et al. [2008] developed a plasma chemical streamer model (hereinafter referred to as S08) to quantify the local chemical effects for a passing sprite streamer at 70 km altitude.

[3] In this paper, we utilize the S08 model with an updated chemical set [Kamaratos, 2009], which is discussed in section 3.2. The modified S08 modeling results are compared to the inferred 762 nm sprite spectroscopic data recorded by the ISUAL experiment. The main purpose of this study is to understand the spectroscopic content of the ISUAL sprites taken through a narrowband 762 nm filter, taking into account the various coupled physical processes producing optical emissions. It is expected that for spaceborne observations, the sprite emissions in the 762 nm range will primarily come from the sprite body due to strong absorption in the O<sub>2</sub> atmospheric band (O<sub>2</sub> atm) by O<sub>2</sub> below 60 km, as indicated by various ground-based measured sprite spectra [Mende et al., 1995; Green et al., 1996; Hampton et al., 1996; Kanmae et al., 2007, 2010]. The 762 nm filter for observing sprites has been proposed for several spacecraft projects, such

<sup>1</sup>Department of Physics, National Cheng Kung University, Tainan, Taiwan.

<sup>2</sup>Earth Dynamical System Research Center, National Cheng Kung University, Tainan, Taiwan.

<sup>3</sup>Physics Department, Pennsylvania State University Lehigh Valley, Center Valley, Pennsylvania, USA.

<sup>4</sup>Institute of Space, Astrophysical and Plasma Sciences, National Cheng Kung University, Tainan, Taiwan.

<sup>5</sup>Geophysical Institute, University of Alaska Fairbanks, Fairbanks, Alaska, USA.

<sup>6</sup>Space Sciences Laboratory, University of California, Berkeley, California, USA.

<sup>7</sup>Department of Cosmochemistry, Hokkaido University, Sapporo, Japan.

<sup>8</sup>Institute of Space Science, National Central University, Jhongli, Taiwan.

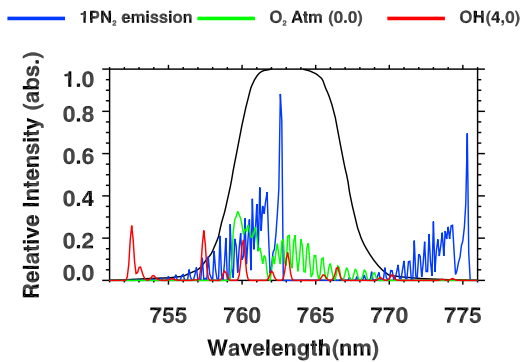


**Figure 1.** The passband of the ISUAL 762 nm imager filter and the emission bands that fall within this passband. The  $1\text{PN}_2$  (2, 0) and (3, 1) bands,  $\text{O}_2$  atmospheric band (0, 0), and OH band (4, 0) emissions are represented by blue, green, and red lines, respectively. The passband of the 762 nm filter is the black line.

as it was used in the narrowband spectroscopic cameras of the SPRITE-SAT project [Takahashi *et al.*, 2010] and in the micro cameras and photometers of the upcoming TARANIS project [Blanc and Lefevre, 2006]. Here, we present spacecraft observations of 762 nm emissions in sprites. The results presented in this paper may be useful to improve the design of the 762 nm filters, in the analysis of sprite 762 nm emissions, and to anticipate possible difficulties that might be encountered in current and future spacecraft observations, especially for the nadir observation of sprites.

## 2. The ISUAL 762 nm Campaign

### 2.1. The Payload and the FORMOSAT-2 TLE Observations

[4] The ISUAL payload on the FORMOSAT-2 satellite consists of an ICCD imager, a six-channel spectrophotometer (SP), and a dual-band array photometer (AP). The images reported here were obtained through a 762 nm filter with an image frame integration time of 29 ms. The 762 nm filter is centered at 763.25 nm with a bandwidth of  $\sim 7$  nm (759.4–767.1 nm at 50% response). The key SP data are from channel 2 (centered at 337 nm; bandwidth 5.6 nm) and channel 3 (centered at 391.4 nm; bandwidth 4.2 nm) of the ISUAL SP. Other SP channels include SP1 (150–290 nm), SP4 (608.9–753.4 nm), SP5 (centered at 777.4 nm for the detection of the lightning OI emissions; bandwidth 7.9 nm), and SP6 (228.2–410.2 nm). The sampling rate of the ISUAL SP is 10 kHz. The ISUAL AP contains blue (370–450 nm) and red (530–650 nm) bands of multiple-anode photometers. Each band of AP has 16 vertically stacked photomultiplier tubes (PMTs) with a combined field of view (FOV) of  $22^\circ$  (H)  $\times$   $3.6^\circ$  (V) [Chern *et al.*, 2003; Mende *et al.*, 2005]. The ISUAL imager, SP and AP are coaligned at the center of their views. The ISUAL imager and SP are bor-sighted, and their FOV is approximately  $20^\circ$  (H)  $\times$   $5^\circ$  (V).

[5] The FORMOSAT-2 is a Sun-synchronous satellite with 14 daily revisiting orbits. The ISUAL payload globally surveys transient luminous events (TLEs) and other luminous emissions in the upper atmosphere with a side-looking view from the 891 km altitude orbit [Chern *et al.*, 2003; Mende

*et al.*, 2005]. Using the satellite information recorded with the TLE events, the altitude and location of the events can be determined by assuming that the bright center of the observed accompanying lightning-illuminated cloud has a height of 10 km [Kuo *et al.*, 2008].

[6] After the ISUAL was launched on 21 May 2004 [Mende *et al.*, 2005], during the first 5 year survey, more than 10,000 TLEs (sprites, halos, elves, and gigantic jets) were recorded by the ISUAL imager through a  $1\text{PN}_2$  filter [Chen *et al.*, 2008; Chou *et al.*, 2010; Chang *et al.*, 2010; Lee *et al.*, 2010]. To study the possible existence of the  $\text{O}_2$  atm band and other emissions falling in the 762 nm passband, a special ISUAL 762 nm imager campaign was conducted from May to August 2008. In this campaign, six elves, two halos and four sprites were recorded by the 762 nm imager.

### 2.2. Sprite Emissions in the 762 nm Passband

[7] Theoretical spectra in Figure 1 indicate that the sprite emissions falling within the 762 nm passband include the first positive bands of molecular nitrogen ( $1\text{PN}_2$ ), the atmospheric band of molecular oxygen, and the hydroxyl (OH) emissions. Figure 1 shows the theoretical rotational-vibrational spectrum of  $1\text{PN}_2$ , which was computed based on the work of Kuo *et al.* [2008]. The assumed rotational temperature, 220 K, is the ambient temperature of the neutral species at 70 km altitude [Brasseur and Solomon, 1986].

[8] The intensity of a  $1\text{PN}_2$  band for a given vibrational level  $v'$  is given by

$$I_{v',v''} = A_{v',v''} N_{v'}, \quad (1)$$

where  $N_{v'}$  is the population of the upper state vibrational level  $v'$  in the band emissions, and  $A_{v',v''}$  is the Einstein coefficient, which is the probability of radiative transition from the upper state vibrational level  $v'$  to the lower state vibrational level  $v''$  [Vallance-Jones, 1974]. In writing (1), it is assumed that the observed  $1\text{PN}_2$  emissions originate well above the quenching altitude of 53 km [Vallance-Jones, 1974], so collisional quenching is not important. The population of the vibrational level  $v'$ ,  $N_{v'}$ , is proportional to the Franck-Condon factor. The Franck-Condon factor is the transition probability from the zeroth vibrational level of the electronic ground state  $\text{N}_2(\text{X}^1\Sigma_g^+)$  to vibrational level  $v'$  of the excited electronic state  $\text{N}_2(\text{B}^3\Pi_g)$ , since the vibrational relaxation time is longer than the lifetime (7  $\mu\text{s}$ ) of the  $1\text{PN}_2$  band above the altitude of 45 km [Kuo *et al.*, 2008, and references therein]. The relative intensities of rotational levels for the  $v'$  vibrational state of  $1\text{PN}_2$  band follow the Boltzmann distribution, and the temperature of the Boltzmann distribution is assumed to be the neutral temperature [Laux, 1993].

[9] The percentage of the total  $1\text{PN}_2$  emissions that fall in the ISUAL imager 762 nm passband is defined as the total  $1\text{PN}_2$  emissions multiplied by the filter response curve. The response function of the 762 nm filter was preflight calibrated and the central wavelength is at 763.25 nm. Using the response curve, the percentage of the total  $1\text{PN}_2$  emissions that fall in the ISUAL 762 nm passband is  $\sim 5\%$ .

[10] The wavelength of the hydroxyl OH (4,0) emissions are computed using the coefficients reported by Meinel [1950] and Herman and Hornbeck [1953]. The population distribution of the vibrational levels for the OH upper state  $\text{X}^2\Pi_{3/2}$  has characteristics of a Boltzmann distribution with

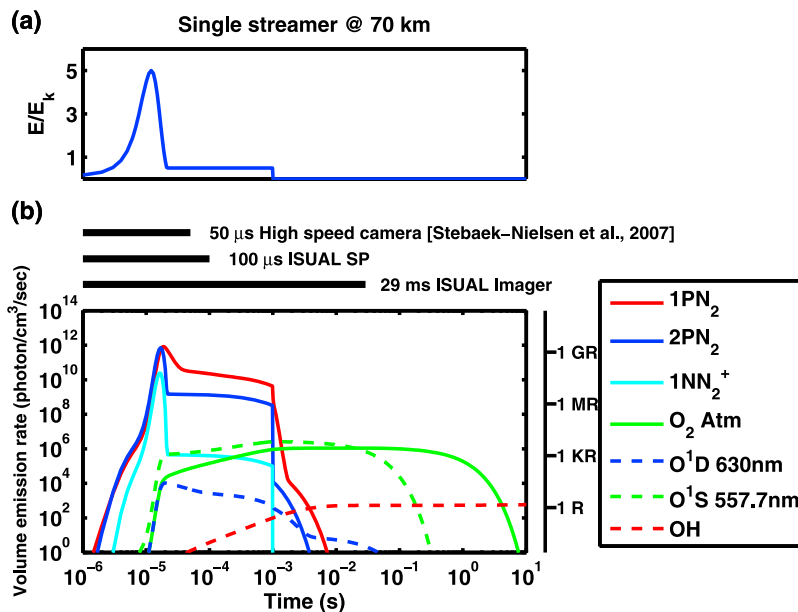


**Figure 2.** The applied electric pulse field and the theoretical brightness of induced band emissions in a sprite streamer. In our plasma chemical model: (a) the maximum applied electric field at streamer tip is  $5 E_k$ , with  $E_k$  being the conventional breakdown electric field, and (b) the volume emission rate (left) and the corresponding brightness (right) for the major band emissions.

$T_v$  of  $\sim 10,000$  K [Khomich *et al.*, 2008, p. 129, and references therein]. The relative population for the vibrational level ( $v' = 4$ ) is  $N_{v'=4} \sim 0.06$ . The ratio of the Einstein coefficient  $A_{4,0}$  to the sum of  $A_{4,v''}$  ( $\sum_{v''} A_{4,v''}$ ) is  $\sim 0.002$  ( $0.13/69.38$ ) [Goldman *et al.*, 1998]. Therefore, the ratio of the OH (4–0) to the total hydroxyl emissions is  $\sim 0.0001$ , which is comparable to the result of  $\sim 0.0002$  derived from the observation data listed by Khomich *et al.* [2008, Table 2.14]. The percentage of the total OH (4,0) emissions that fall in the passband of the ISUAL 762 nm filter is 28%. Hence, the percentage of the total OH emissions in the 762 nm filter is  $\sim 0.003\%$  ( $0.0001 \times 28\%$ ), which is small enough to be neglected.

[11] The intensity of the  $O_2$  atm (0,0) rotational spectrum is computed using the information provided by Babcock and Herzberg [1948] and is shown as the green curve in Figure 1. The intensity ratio of  $O_2$  atm (0,0) to the total  $O_2$  atm emission band is 88.5% [Khomich *et al.*, 2008, Table 2.27]. The percentage of the total  $O_2$  atm (0,0) emissions that fall in the ISUAL 762 nm passband is  $\sim 84.6\%$ . The expected percentage of the detectable  $O_2$  atm (0,0) from the total  $O_2$  atm band emissions is therefore  $\sim 75\%$  ( $88.5\% \times 84.6\%$ ).

### 2.3. Absorption of $O_2(b^1\Sigma_g^+) \rightarrow O_2(X^3\Sigma_g^-)$

[12] The oxygen density profile between the altitudes of 0 km to 1000 km is obtained from the MSIS model [Hedin, 1991]. This density profile is useful in computing the column integrated molecular oxygen density, which is responsible for the absorption of 762 nm emissions by the oxygen along the raypaths that connect the ICCD imager and the TLEs. For the sprite event on 15 May 2008, 2157:30.446, the event location is determined to be  $\sim 7^\circ N$  and  $15^\circ E$ . Since the absorption cross section of molecular nitrogen is very small [Jursa, 1985, p. 22–4], the molecular nitrogen absorption of the 762 nm emissions can be neglected. The column

integrated molecular oxygen density is  $2.1 \times 10^{21}$  molecules  $cm^{-2}$ , and the absorption cross sections at the peaks of the P (760.8 nm) and the R (763.8 nm) branches of the  $O_2(b^1\Sigma_g^+) \rightarrow O_2(X^3\Sigma_g^-)$  emissions are  $3.2 \times 10^{-24}$  and  $2.2 \times 10^{-24}$   $cm^2$  [Greenblatt *et al.*, 1990], respectively. Using the Lambert's law, the atmospheric transmittance can be expressed as  $e^{-L(h,d,\lambda)\sigma(\lambda)}$  where  $L(h, d, \lambda)$  is the column integrated molecular oxygen density as a function of altitude ( $h$ ), distance ( $d$ ), and wavelength ( $\lambda$ ); the laboratory-measured cross section  $\sigma(\lambda)$  is in units of  $cm^2$ . The transmittances for sprite emissions at wavelengths of 760.8 and 763.8 nm from an altitude of 70 km and at a distance of 2800 km are 99.3% and 99.5%, respectively. Therefore, the absorption percentage of the 762 nm emissions from the sprite on 15 May 2008, 2157:30.446 at 70 km altitude is less than 1%.

## 3. The Plasma Chemistry Model for a Sprite Streamer

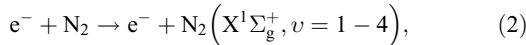
### 3.1. The Zero-Dimensional Plasma Chemistry Model

[13] A zero-dimensional plasma chemistry model was first developed by Sentman *et al.* [2008] to study the localized chemical reactions induced by the electric discharges associated with sprite streamers over a wide range of timescales, and the associated radiative emissions. The timescales span several orders of magnitude from  $\mu s$  to tens of seconds. Taking the ionization pulse depicted in Figure 2a as an example, the pulse length is assumed to be 100 m and the propagation speed is  $\sim 10^7$   $m s^{-1}$  [McHarg *et al.*, 2007; Stenbaek-Nielsen *et al.*, 2007; Li and Cummer, 2009], hence a fixed point in the streamer head will experience  $\sim 10 \mu s$  of transient E field. Though the driving electric field only lasts for 10  $\mu s$ , the induced plasma chemical reactions can continue for several seconds. Within the passband of the 762 nm filter,

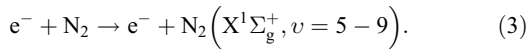
the radiative lifetime of the 1PN<sub>2</sub> emissions (5.4 μs) is found to be about six orders of magnitude shorter than that for the O<sub>2</sub> atm band (~12 s). The applicable temporal window of the S08 model can span from microseconds to tens of seconds. Hence, the relative radiative intensities of the sprite streamer emissions, including 1PN<sub>2</sub>, 1NN<sub>2</sub><sup>+</sup>, O<sub>2</sub> atm and OH band emissions, can be traced over a wide range of timescales.

### 3.2. The Chemical Reaction Set in the Plasma Chemistry Model

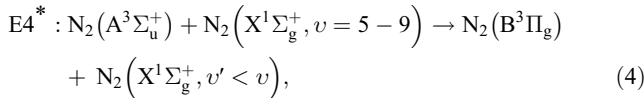
[14] In this work, the basic chemical reaction set and species of S08 are adopted with the inclusion of additional modifications that were discussed by *Kamaratos* [2009]. For example, *Kamaratos* [2009] suggested that the following electron impact processes should be considered for the lower vibrational states of N<sub>2</sub> (X<sup>1</sup>Σ<sub>g</sub><sup>+</sup>, *v* = 1 – 4),



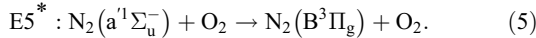
and for the higher vibrational states of N<sub>2</sub>(X<sup>1</sup>Σ<sub>g</sub><sup>+</sup>, *v* = 5 – 9),



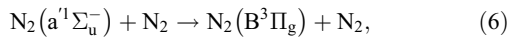
[15] The following vibrational kinetics is also considered [*Kamaratos*, 2009],



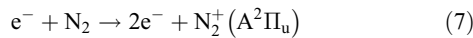
where the chemical reaction rate constant is  $4 \times 10^{-11} \text{ cm}^3 \text{ molecules}^{-1} \text{ s}^{-1}$  [*Piper*, 1992, 1994]. Also, the following reaction is added as discussed in [*Kamaratos*, 2009],



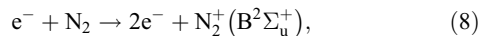
[16] The rate of this chemical reaction constant is  $3.2 \times 10^{-11} \text{ cm}^3 \text{ molecules}^{-1} \text{ s}^{-1}$  [*Umemoto et al.*, 2003]. In addition, the reaction rate constant of the following reaction is changed:



to be 0.02 times the value given in S08 model [*Kamaratos*, 2009], thus is  $4 \times 10^{-15} \text{ cm}^3 \text{ molecules}^{-1} \text{ s}^{-1}$ . Finally, for species N<sub>2</sub><sup>+</sup>(A<sup>2</sup>Π<sub>u</sub>) and N<sub>2</sub><sup>+</sup>(B<sup>2</sup>Σ<sub>u</sub><sup>+</sup>) and the processes

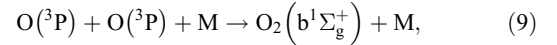


and



the branching ratios are specified to be 0.535 and 0.145 times of the N<sub>2</sub> ionization ( $e^- + N_2 \rightarrow 2e^- + N_2^+$ ) by *Van Zyl and Pendleton* [1995], respectively. Therefore, the reaction rate constants for reactions (7) and (8) are 0.535 and 0.145 times that of the N<sub>2</sub> ionization rate ( $e^- + N_2 \rightarrow 2e^- + N_2^+$ ). The electron impact ionization processes, reactions (7) and (8), are used for estimating the emission intensity of the N<sub>2</sub><sup>+</sup> Meinel band and the N<sub>2</sub><sup>+</sup> first negative band (1NN<sub>2</sub><sup>+</sup>) emissions. For

the O<sub>2</sub> atm band emissions, a two-step Barth-type process, a three-body recombination reaction, [*McDade et al.*, 1986; *Marsh et al.*, 2002; *Belyaev et al.*, 2006] is considered,



where *M* either is molecular nitrogen or oxygen. The rate constant for (9) is  $\sim \varepsilon \times 4.7 \times 10^{-33} (300/T)^2$  where *T* is the temperature (in Kelvin) and the coefficient  $\varepsilon \sim 0.1$  since the number ratio of O<sub>2</sub>(b<sup>1</sup>Σ<sub>g</sub><sup>+</sup>) to all the O<sub>2</sub> substates from the total recombination reaction [*McDade et al.*, 1986] is  $\sim 0.1$ . For OH emissions, the relevant chemical reactions are included in the S08 model [*Sentman et al.*, 2008].

## 4. Model Results and the Observed Sprite 762 nm Emissions

### 4.1. Major Emissions in a Sprite Streamer

[17] Figure 2a shows the magnitude and duration of an impulsive E field moving along the symmetrical axis of a streamer from the streamer head moving toward the streamer body. The E field within the streamer is parameterized as the following:

$$\text{the streamer head } (t < 18\mu\text{s}), \quad (10a)$$

$$E(t) = E_h e^{-(t-t_0)^2/\Delta t^2} \quad t < t_0 + 3\Delta t,$$

and the streamer body ( $t > 18 \mu\text{s}$ ),

$$E(t) = E_b \quad t_0 + 3\Delta t \leq t \leq 1\text{ms}, \quad (10b)$$

where a high electric field at the streamer head lasts for  $\Delta t = 6 \mu\text{s}$  and a small E field in streamer body is assumed to persist for  $\sim 1 \text{ ms}$ . These times are estimated values from assuming that the length of a streamer is  $\sim 10 \text{ km}$  and the ionization wave at the streamer head moves at a speed of  $10^7 \text{ m/s}$  [*McHarg et al.*, 2007; *Stenbaek-Nielsen et al.*, 2007; *Li and Cummer*, 2009]. The peak magnitudes of the E field are  $E_h = 5 E_k$  at the streamer head and  $E_b = 0.5 E_k$  in streamer body, respectively. Here,  $E_k$  is the conventional breakdown E field and is equal to  $\sim 220 \text{ V/m}$  at altitude 70 km where the air density is  $1.5 \times 10^{15} \text{ molecules cm}^{-3}$ . The adopted  $E_b$  and  $E_h$  values are similar to those used in the modeling of positive streamer propagating in the background E field  $\sim E_k$  [*Liu et al.*, 2009a, 2009b] and in the plasma chemical streamer model reported by *Sentman and Stenbaek-Nielsen* [2009].

[18] The computed major optical emissions in a streamer are shown in Figure 2b, and the density evolution of the major chemical species in a single streamer is shown in Figure 3. The dominant emissions (1PN<sub>2</sub>, 2PN<sub>2</sub>, 1NN<sub>2</sub><sup>+</sup> and N<sub>2</sub><sup>+</sup> Meinel) in a streamer are primarily from the electron impact excitations within the streamer head region. The streamer radius is assumed to be 25 m [*Sentman et al.*, 2008], the computed peak photon emission rate of 1PN<sub>2</sub> is  $8.4 \times 10^{11} \text{ photons cm}^{-2} \text{ s}^{-1}$ , and the corresponding peak 1PN<sub>2</sub> brightness is  $2.5 \times 10^3 \times 8.4 \times 10^{11} \sim 2 \times 10^9 \text{ Rayleigh}$  (2 GR) where 1 Rayleigh =  $10^6 \text{ photons s}^{-1}$  in a 1 cm<sup>2</sup> column. The 2PN<sub>2</sub>, 1NN<sub>2</sub><sup>+</sup> and N<sub>2</sub><sup>+</sup> Meinel emissions are 1.8 GR, 0.06 GR and 0.044 GR at the streamer head, respectively. The brightness of the streamer body is nearly two orders of magnitude lower than the brightness of the streamer head.

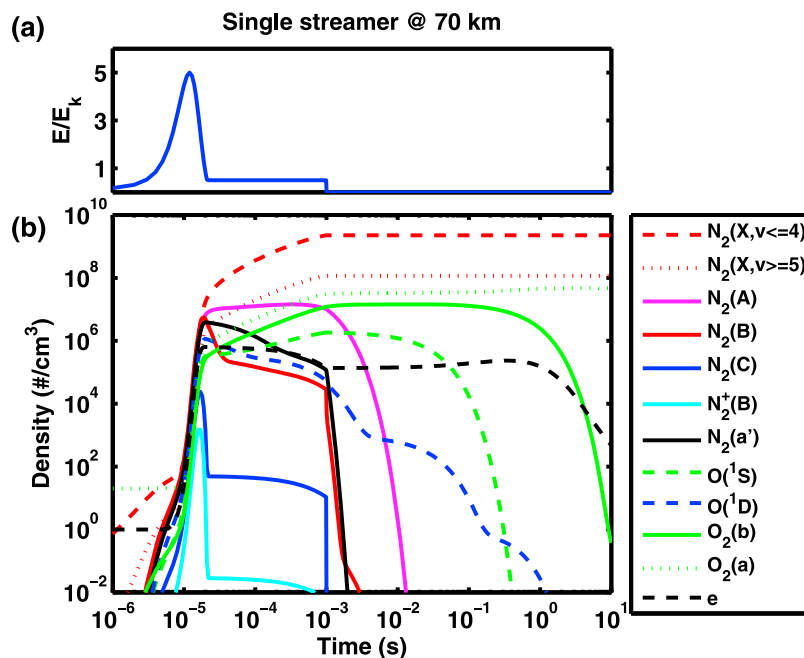


**Figure 3.** The dominant chemical species along the symmetrical axis of a single streamer: (a) the applied electric pulse field and (b) the number density evolution.

The brightness of  $1PN_2$ ,  $2PN_2$ ,  $1NN_2^+$  and  $N_2^+$  Meinel emissions are estimated to be 24 MR, 1.8 MR, 2.1 kR and 0.6 kR in the streamer body, respectively.

[19] Even with a relatively low E field at the streamer body ( $E_b = 0.5 E_k$ ), the radiative contribution from the electron impact excitations in the streamer body is only two orders of magnitude less than that from the emissions at the streamer head. After the removal of E field ( $E_b = 0$ ), the  $1PN_2$ ,  $2PN_2$ , and  $1NN_2^+$  emissions decay immediately. The induced emissions, including  $O_2$  atm,  $O(^1D)$  630 nm,  $O(^1S)$  557.7 nm and OH emissions, are produced by species lasting for more than 1 ms. The maximum brightness for the  $O_2$  atm emissions is 2.6 kR at 2 ms,  $O(^1D)$  630 nm is 30 R at 20  $\mu$ s,  $O(^1S)$  557.7 nm is 6.5 kR at 1 ms, and OH emissions is 1.5 R after 1 s. One reason for the long lifetime of these emissions compared to those for electron impact excited emissions is the

smallness of their radiative Einstein coefficients. Another reason is that the chemical reaction rates for producing the minor species are slow. Table 1 shows the transition, the wavelength, and the radiative Einstein coefficients for the major band emissions in a model sprite streamer.

#### 4.2. The Chemical Reactions Leading to the $O_2$ Atmospheric Band Emissions

[20] The possible pathways to generate the observed 762 nm emissions are discussed here, and the results are depicted in Figure 4. Figure 4a depicts the profile of the electric field in a sprite streamer. Figure 4b presents the number density of the  $O_2$  ( $b^1\Sigma_g^+$ ) substate, which is the upper state of the  $O_2$  atm band. Figure 4c shows the temporal evolution of the related chemical reactions that lead to the production and the loss of  $O_2$  ( $b^1\Sigma_g^+$ ), which are indicated by

**Table 1.** Major Band Emissions of Sprite Streamers, the Upper and Lower States, the Emission Wavelengths, the Einstein Coefficients ( $A_k$ ), and the Quenching Constants ( $K_q$ ) for Molecular Nitrogen and Oxygen

Emission Band System	Upper and Lower States	Wavelength (nm)	$A_k$ ( $s^{-1}$ )	$K_q, N_2$	$K_q, O_2$
$1PN_2$	$N_2(B^3\Pi_g) \rightarrow N_2(A^3\Sigma_u^+)$	478–2531	$1.7 \times 10^{4a}$	$1.60 \times 10^{-11b}$	$1.50 \times 10^{-10b}$
$2PN_2$	$N_2(C^3\Pi_u) \rightarrow N_2(B^3\Pi_g)$	268–546	$2.0 \times 10^{7c}$	$1.12 \times 10^{-11d}$	$2.85 \times 10^{-10d}$
$1NN_2^+$	$N_2^+(B^2\Sigma_u^+) \rightarrow N_2^+(X^2\Sigma_g^+)$	286–587	$1.6 \times 10^{7a}$	$4.53 \times 10^{-10d}$	$7.36 \times 10^{-10d}$
$O_2$ atmosphere	$O_2(b^1\Sigma_g^+) \rightarrow O_2(X^3\Sigma_g^-)$	538–997	$7.7 \times 10^{-2e}$	$2.10 \times 10^{-15f}$	$1.00 \times 10^{-16f}$
O	$O(^1S) \rightarrow O(^3P)$	557.7	1.43		$3.00 \times 10^{-13c}$
O	$O(^1D) \rightarrow O(^3P)$	630	$9.10 \times 10^{-3}$	$5.00 \times 10^{-11f}$	$5.50 \times 10^{-11f}$
OH	$X^2\Pi_{3/2} \rightarrow X^2\Pi_{1/2}$	500–5000	$2.18 \times 10^{2g}$	$1.00 \times 10^{-13g}$	$1.00 \times 10^{-13g}$

<sup>a</sup>Based on a private discussion [Liu and Pasko, 2005], the middle value of Einstein coefficient for major vibrational levels of upper state of band system [Gilmore et al., 1992, Table 19] is used in our model.

<sup>b</sup>Piper [1992].

<sup>c</sup>The lower Einstein coefficient [Vallance-Jones, 1974, p. 119] provides a better fit for our observation and is 74% of that listed by Gilmore et al. [1992, Table 19].

<sup>d</sup>With these values, the quenching height for  $2PN_2$  and  $1NN_2^+$  are  $\sim 30$  and  $\sim 48$  km [Pancheshnyi et al., 1997].

<sup>e</sup>Vallance-Jones [1974].

<sup>f</sup>Sander et al. [2003] and Slanger and Copeland [2003].

<sup>g</sup>Sentman et al., 2008, and references therein.

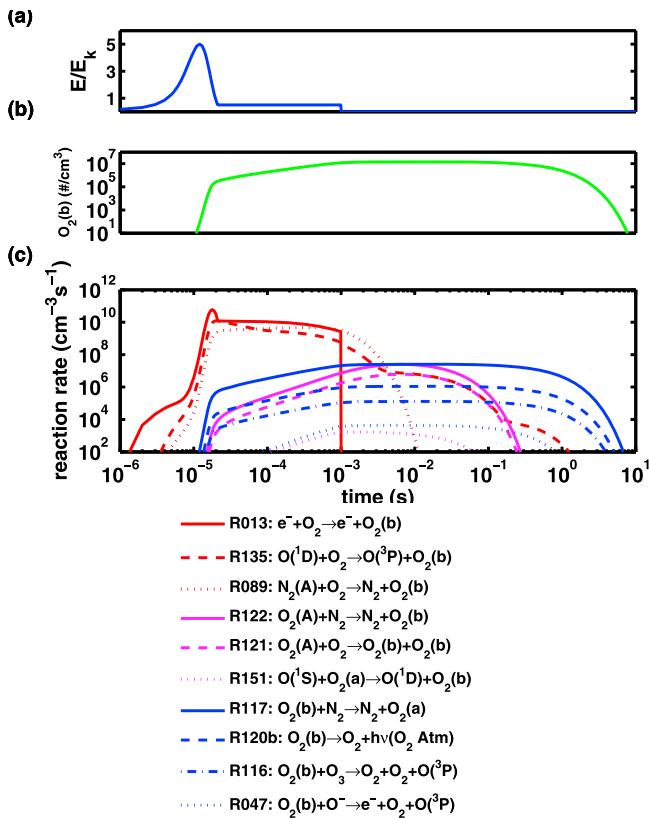


**Figure 4.** The chemical reactions leading to the  $O_2$  atmospheric band emissions. (a) The applied electric field; the maximum electric field at the streamer tip is  $5 E_k$ . (b) The accumulated density of the  $O_2(b^1\Sigma_g^+)$  upper state of the  $O_2$  atmospheric bands. (c) The chemical reaction rate for the production and the loss of the  $O_2(b^1\Sigma_g^+)$  upper state. The reaction labels are the same as given in Appendix A of *Sentman et al.* [2008].

red and blue curves, respectively. The dominant reaction for the production of  $O_2(b^1\Sigma_g^+)$  is via an electron impact reaction; R13 in Figure 4c. These reactions are all resulting from the driving electric field as shown in Figure 4 or from the active species left behind in the streamer head and the streamer body regions after 1 ms. The electric field driven chemical processes reach their peaks at  $\sim 10 \mu\text{s}$ , e.g., R13, R135 and R89 (designations refer to chemical reaction numbers in Appendix A of S08), and decay rapidly after the electric field was switched off after 1 ms. The  $O(^1D)$  in R141b has a relatively long radiative lifetime of  $\sim 110$  s, as listed in

Table 1. Hence, the reaction rate of R141b has the second highest peak after 1 ms, whereas the highest reaction rate comes from the chemical reaction R122. After the electric field was switched off, the chemically active species in the streamer region are  $O(^1D)$  in R135, metastable  $O_2(A)$  in R121 and R122, and  $O(^1S)$  in R151. Their reaction rates peak after  $\sim 10$  ms, the same as for the number density of the  $O_2(b^1\Sigma_g^+)$ . This indicates that chemical processes associated with active species  $O(^1D)$  in R135 and  $O_2(A)$  in R121 and R122 make a significant contribution to the production of  $O_2(b^1\Sigma_g^+)$ , the upper state of  $O_2$  atm band.

[21] The chemical reactions responsible for the loss of  $O_2(b^1\Sigma_g^+)$  include the collisional deactivation processes R117, the radiation reaction R120b, and active state chemistry R116 and detachment processes R47; see Figure 4. The dominant loss chemical process is the quenching process R117, while the second highest is from radiation reaction R120b. The radiative lifetime of  $O_2(b^1\Sigma_g^+)$  is  $\sim 12$  s, as listed in Table 1. The chemical reactants involved in these loss reactions are  $N_2$  in R117,  $O_3$  in R116, and  $O^-$  in R47. The reactions rates of the chemical loss reactions control the  $1/e$  reduction time of  $O_2(b^1\Sigma_g^+)$  where the  $1/e$  reduction time is defined as the time for the  $O_2(b^1\Sigma_g^+)$  population to drop to  $1/e$  of the maximum value, and they also define the luminous time of the  $O_2$  atm band. As indicated in Figure 4b, the  $1/e$  reduction time of  $O_2(b^1\Sigma_g^+)$  is  $\sim 0.6$  s, thus the luminous time of the  $O_2$  atm band can last  $\sim 1$  s as it can be inferred from Figure 3b.

### 4.3. Comparison of the Model and the Observed Streamer Emissions

[22] Here we compare the model emissions, the observed sprite streamer emissions reported by *Stenbaek-Nielsen et al.* [2007] and *Stenbaek-Nielsen and McHarg* [2008] and those from the sprite streamer model [*Liu and Pasko*, 2004, 2005; *Liu et al.*, 2009a, 2009b]. These data are tabulated in Table 2. From sprite observations reported by *Stenbaek-Nielsen et al.* [2007] and *Stenbaek-Nielsen and McHarg* [2008], the measured brightness of sprites is  $4 \times 10^8 - 3 \times 10^{11}$  Rayleigh in an ICCD camera with exposure time of  $50 \mu\text{s}$ . Thus, the corresponding photon emission rate in the streamer head is  $10^{21} - 3 \times 10^{24}$  photons  $\text{s}^{-1}$  [*Stenbaek-Nielsen et al.*, 2007].

[23] In our model, the assumed streamer diameter 25 m is comparable to what was observed and that used in the streamer model. The average photon emission rate in an ICCD camera with exposure time  $50 \mu\text{s}$  is  $\sim 10^{11}$  photons  $\text{cm}^{-3} \text{s}^{-1}$ . The volume of a streamer head is on the order of  $\sim 25^3 \text{ m}^3 = 1.5 \times 10^{10} \text{ cm}^3$ . The model photon rate in streamer head is  $\sim 10^{11}$  photons  $\text{cm}^{-3} \text{s}^{-1} \times 1.5 \times 10^{10} \text{ cm}^3 =$

**Table 2.** Intensity of Sprite Streamer Emissions From This Work, the Observation Reported by *Stenbaek-Nielsen et al.* [2007], and the Streamer Model<sup>a</sup>

	Sprite Observation <sup>b</sup>	This Model ( $E_h = 5 E_k, E_b = 0.5 E_k$ )	Streamer Model <sup>c</sup>
Altitude	75 km	70 km	70 km
IPN <sub>2</sub>			
Brightness (Rayleigh)	$4 \times 10^8$ to $3 \times 10^{11}$	$2.5 \times 10^8$	$10^7$ (weak field) to $5 \times 10^8$ (strong field)
Photon flux (photons $\text{cm}^{-2} \text{s}^{-1}$ )	$3 \times 10^5$ to $>2 \times 10^8$	$2.2 \times 10^6$	

<sup>a</sup>The modeled and the observed emissions are from the streamer tips, and the modeled photon fluxes are computed using the event distances reported by *Stenbaek-Nielsen et al.* [2007].

<sup>b</sup>*Stenbaek-Nielsen et al.* [2007].

<sup>c</sup>*Liu and Pasko* [2004, 2005].

**Table 3.** The Emission Ratios of  $2\text{PN}_2/1\text{PN}_2$  and  $2\text{PN}_2/1\text{INN}_2^+$  in Sprites From the ISUAL Observed Events, This Model, and the Streamer Model Reported by *Liu et al.* [2006, 2009a, 2009b]<sup>a</sup>

	ISUAL Recorded Sprites <sup>b</sup>	This Model; in Streamer Head Region	Streamer Model <sup>c</sup>
$2\text{PN}_2/1\text{PN}_2$	$0.24 \pm 0.04$	$0.37 (E_h = 3\text{--}5 E_k)$	0.47
$2\text{PN}_2/1\text{INN}_2^+$	$32.2 \pm 11.2$	$36.3 (E_h \sim 3 E_k), 30.7 (E_h \sim 5 E_k)$	$\sim 40$ (weak field, $E_h \sim 3 E_k$ ), $\sim 30$ (strong field, $E_h \sim 5 E_k$ )

<sup>a</sup>It should be noted that the observed ratios are computed using the time-integrated emissions from all regions of sprites, while the model values are from a single sprite streamer.

<sup>b</sup>*Kuo et al.* [2005].

<sup>c</sup>*Liu et al.* [2006, 2009a, 2009b].

$1.5 \times 10^{21}$  photons  $\text{s}^{-1}$ . Therefore, the estimated brightness is  $10^{11}$  photons  $\text{cm}^{-3} \text{s}^{-1} \times 25 \text{ m} = 2.5 \times 10^{14}$  photons  $\text{cm}^{-2} \text{s}^{-1} = 2.5 \times 10^8$  Rayleigh. The brightness reported in the streamer modeling [*Liu and Pasko*, 2004, 2005; *Liu et al.*, 2009a, 2009b] is  $10^7$  Rayleigh for a weak electric field case and  $5 \times 10^8$  Rayleigh for a strong electric field case.

[24] Assuming a constant emission rate for a streamer head with a propagation velocity  $10^7 \text{ m s}^{-1}$ , the spatially integrated photons during  $50 \mu\text{s}$  is  $\sim 25 \text{ m} \times 25 \text{ m} \times (10^7 \text{ m s}^{-1} \times 50 \mu\text{s}) \times 10^{11} \text{ photons cm}^{-3} \text{s}^{-1} = 3.1 \times 10^{22}$  photons  $\text{s}^{-1}$ . Assuming isotropic emissions and an estimated sprite distance of 335 km as reported by *Stenbaek-Nielsen et al.* [2007], the photon flux is  $3.1 \times 10^{22} \text{ photons s}^{-1} / 4\pi / (3.35 \times 10^7 \text{ cm})^2$ , or  $2.2 \times 10^6 \text{ photons cm}^{-2} \text{s}^{-1}$ . These model-derived parameters are all consistent with the observed values in sprite streamers [*Stenbaek-Nielsen et al.*, 2007; *Stenbaek-Nielsen and McHarg*, 2008].

[25] Analyzing five ISUAL recorded sprites, *Kuo et al.* [2005, Table 3] reported that, within the spectrophotometer 0.1 ms integration window, the emission ratios for  $2\text{PN}_2/1\text{INN}_2^+$  and  $2\text{PN}_2/1\text{PN}_2$  are  $32.2 \pm 11.2$  and  $0.24 \pm 0.04$ , respectively. Comparing the model results in this work and those reported by *Liu and Pasko* [2004, 2005] and *Liu et al.* [2009a, 2009b], the estimated emission ratios for  $2\text{PN}_2/1\text{INN}_2^+$  and  $2\text{PN}_2/1\text{PN}_2$  are consistent and are listed in Table 3. This model work and the streamer model of *Liu and Pasko* [2004, 2005] and *Liu et al.* [2009a, 2009b] are for a single streamer, while the ISUAL SP recorded  $1\text{PN}_2$ ,  $2\text{PN}_2$  and  $1\text{INN}_2^+$  emissions are spatially integrated over all the streamers in sprites. Nevertheless, it is expected that the model results for a single streamer can be generalized and applicable to the whole sprite.

#### 4.4. The Intensity Ratio of the Sprite $1\text{PN}_2$ and the $\text{O}_2$ Atmospheric Band Emissions

[26] To infer the relative emission intensity of the  $\text{O}_2$  atm and the  $1\text{PN}_2$  in sprites, we use the model intensities to evaluate the brightness of the emission bands in the 762 nm filter. Figure 5 shows the averaged brightness of the major sprite emission bands for six temporal bins of 30 ms each. The temporal length and the bin size are chosen to match the frame integration time and the six-frame recording length of the ISUAL imager. The estimated  $1\text{PN}_2$ ,  $2\text{PN}_2$  and  $1\text{INN}_2^+$  brightness are 1.4 MR, 0.3 MR and 6.7 kR, respectively, for the first frame. As shown in Figure 2, the luminous duration ( $\sim 1$  ms) of these band emissions is substantially shorter than the integration time (30 ms) of a single imager frame; see Figure 6. The model results indicate that the maximum brightness of the  $\text{O}_2$  atm band,  $\text{O}(^1\text{D})$  630 nm,  $\text{O}(^1\text{S})$  557.7 nm and OH emissions is  $\sim 2.6$  kR,  $\sim 0.6$  R,  $\sim 3.6$  kR and  $\sim 1.3$  R, respectively. Since the chemical reactions leading to

the  $\text{O}_2$  atm band emissions have a lifetime of  $\sim 12$  s as discussed in section 4.2, the  $\text{O}_2$  atm band emissions last and remain nearly constant over six imager frames of 180 ms. The average brightness of the  $\text{O}_2$  atm band emissions is  $\sim 2.6$  kR as can be inferred from Figure 5.

[27] Table 4 summarizes the model brightness for the emissions  $1\text{PN}_2$ ,  $\text{O}_2$  atm and OH in the passband (759.4–767.1 nm) of the 762 nm filter. The model brightness for these emission bands at the 30 ms integration time is listed in the second column of the Table 4, after correction for the detection percentage through the 762 nm passband (see discussions in section 2.4). The estimated  $1\text{PN}_2$  and  $\text{O}_2$  atm brightness in the 762 nm filter are 70 kR and 2 kR, respectively. The brightness ratio of  $1\text{PN}_2$  to  $\text{O}_2$  atm is  $\sim 35$ . Therefore, it is generally difficult to distinguish the weaker  $\text{O}_2$  atm (0, 0) emissions from the dominant  $1\text{PN}_2$  band emissions. However, the luminous duration of the  $\text{O}_2$  atm band can be up to 1 s, which is much longer than that for the  $1\text{PN}_2$ . Therefore to resolve and confirm the existence of the 762 nm  $\text{O}_2$  atm (0, 0) emissions, ISUAL recorded sprite emissions beyond the first frame (30 ms) have to be analyzed in detail.

#### 4.5. The ISUAL 762 nm Sprites

[28] Figure 6 shows the ISUAL 762 nm imager frames and the associated AP data for a sprite recorded on 15 May 2008, 2157:30.446. The time tags above each image frame denote the beginning times of these 29 ms frames relative to the event trigger. The time resolution of AP is 0.05 ms in the first 10 ms after the event trigger. From the emission profile of the ISUAL AP blue and red modules, the initiation point for this

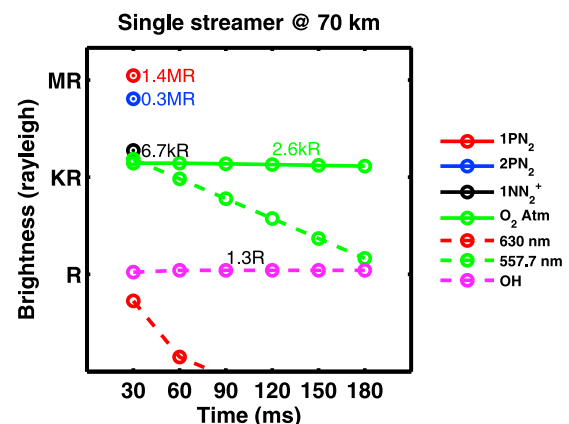


**Figure 5.** The model brightness of major emission bands for a streamer at altitude of 70 km and with a exposure time of 30 ms. The choice of the exposure time is to close match that of the ISUAL 29 ms imager frame.

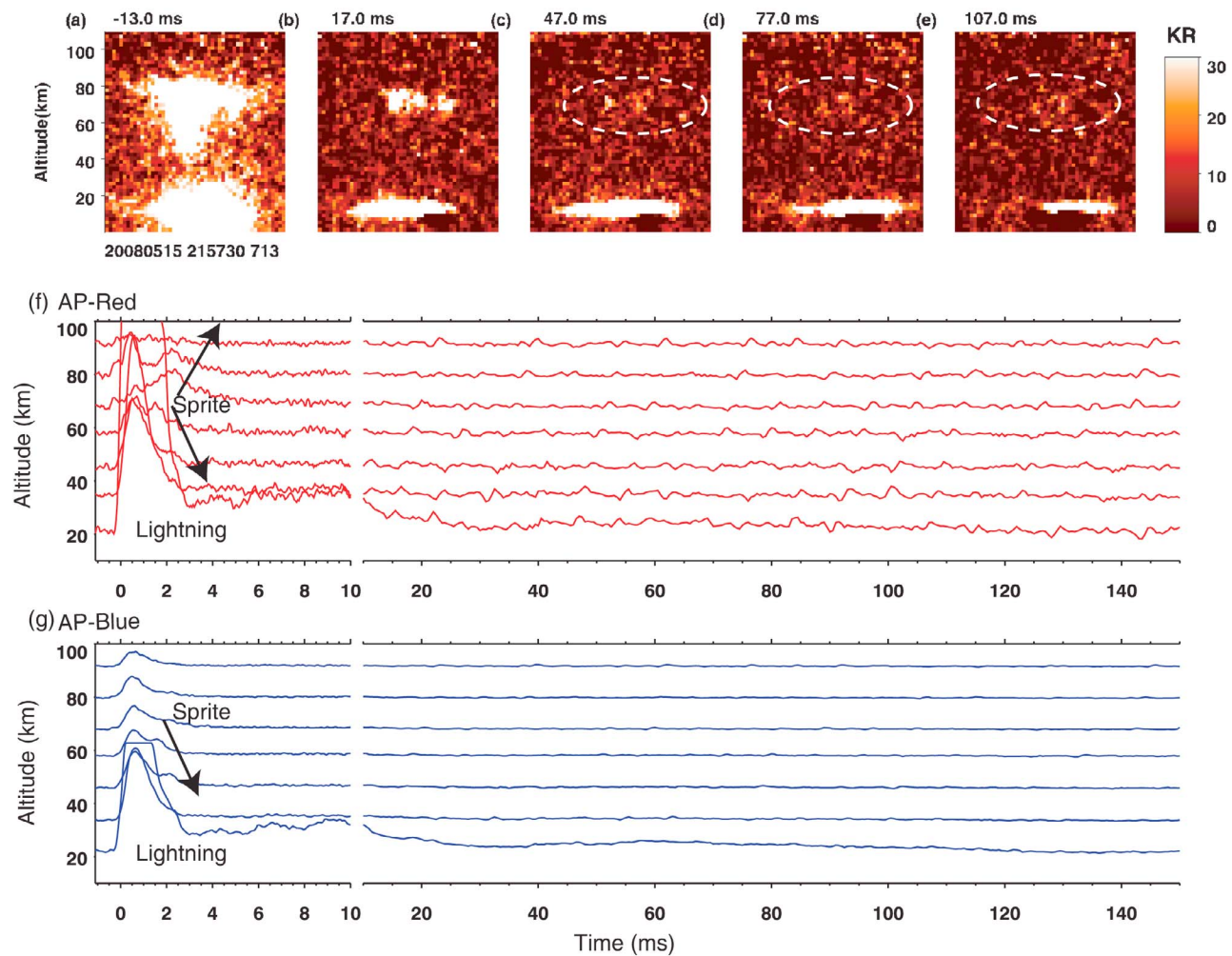


**Figure 6.** The ISUAL imager and array photometer data for the 762 nm sprite on 15 May 2008, 2157:30.446. (a–e) The first five imager frames of this event. The white ovals denote the regions that contain the O<sub>2</sub> atmospheric band (0, 0) emissions. (f and g) The red and the blue band photometric data from the array photometers.

sprite is determined to be between 58 and 70 km. The sprite initiation time was  $\sim 1.5$  ms after the trigger from AP data.

[29] From Figures 6a–6e, this 762 nm sprite seems to contain two types of emissions. The first type is the primary emissions, and they are so relatively short-lived that they only show up in the first two frames of Figure 6. The average brightness of this sprite in frames a and b is  $\sim 173$  kR, and the maximum brightness is  $\sim 1$  MR. The second type is weak continuous emissions that persist into frames c, d and e, as may be discerned in Figure 6. The second group of emissions

could have begun from the first frame and have persisted for more than 90 ms. The maximum brightness for the persisting emissions in frames c, d, and e are 28.6, 27.6, 23.3 kR, respectively. The recorded O<sub>2</sub> atm (0, 0) in the sprite is estimated to be  $\sim 30$  kR, while its 1PN<sub>2</sub> brightness is  $\sim 1$  MR. Hence for this sprite, the brightness of this persisting emissions is about 1/33 that of the 1PN<sub>2</sub> in the 762 nm passband, which is consistent with the model predicted value of 1/35 (see section 4.4). The only significant emissions that could exist in the temporal range is the O<sub>2</sub> atm (0, 0) emissions,

**Table 4.** The 1PN<sub>2</sub>, O<sub>2</sub> Atmospheric Band (0, 0) and OH Band (4, 0) Emissions From a Sprite Streamer That Fall Within the ISUAL 762 nm Filter Passband<sup>a</sup>

	Modeled Brightness of Total Emission Bands	Detected Percentage	Estimated Brightness	Brightness Ratio
1PN <sub>2</sub>	1.4 MR	$\sim 5\%$	70 kR	1
O <sub>2</sub> atm (0, 0)	2.6 kR	$\sim 75\%$	2 kR	$\sim 0.03$
OH (4, 0)	1.3 R	0.003%	0.004 R	$\sim 7 \times 10^{-8}$

<sup>a</sup>The columns present the theoretical emission band brightness from our plasma chemistry model, the percentage of the band emissions that fall within the ISUAL 762 nm filter, the predicted brightness in the 762 nm passband, and the estimated brightness ratio if a single streamer can correctly reflect the ratio of the whole sprite.

whose parent chemical reaction has a lifetime of  $\sim 12$  s. Hence it can be concluded that the persisting 762 nm emissions in this sprite is from the  $O_2$  atm (0, 0) band.

[30] Among the four sprites recorded by the ISUAL imager through the 762 nm filter, only the brightest event analyzed above has discernible  $O_2$  atm (0, 0) emissions. The other three sprite events either are too dim, or were recorded in the penultimate imager frame and the  $O_2$  atm (0, 0) emissions are swarmed by the dominant  $1PN_2$  emissions, thus they cannot be resolved.

## 5. Discussion

[31] The minor differences between the plasma chemical model employed here and that by *Sentman et al.* [2008] lie in the slightly different sets of chemical equations used in the respective works. In the present work, the reactions (2)–(6) associated with the excited species  $N_2(a^1\Sigma_u^-)$  and the  $N_2$  vibrational kinetics were included, as suggested by *Kamaratos* [2009] and references therein.

[32] The dominant process in producing  $N_2(B^3\Pi_g)$  is the cascading process  $N_2(C^3\Pi_u) \rightarrow N_2(B^3\Pi_g) + h\nu$  ( $2PN_2$ ). The radiative life time of this cascading process is very short, 50 ns, which is the inverse of the corresponding Einstein coefficient listed in Table 1. However, after the production of  $N_2(a^1\Sigma_u^-)$ , the quenching collisions with  $O_2$  or  $N_2$  can cross  $N_2(a^1\Sigma_u^-)$  into  $N_2(B^3\Pi_g)$  and cause an enhancement of the  $1PN_2$  emissions [*Kamaratos*, 2009, and references therein]. In our model single streamer, the maximum density of the excited species  $N_2(a^1\Sigma_u^-)$  can be up to  $3.8 \times 10^6 \text{ cm}^{-3}$ ,  $\sim 67\%$  of the maximum density ( $5.6 \times 10^6 \text{ cm}^{-3}$ ) of  $N_2(B^3\Pi_g)$ ; Figure 3.

[33] That affect the excited species  $N_2(a^1\Sigma_u^-)$  are the radiative transition (Ogawa-Tanaka-Wilkinson-Mulliken band system,  $a^1\Sigma_u^- - X^1\Sigma_g^+$ ) [*Lofthus and Krupenie*, 1977], the production of two O atoms [*Kossyi et al.*, 1992], the quenching processes with  $N_2$  and  $O_2$  [*Umamoto et al.*, 2003], and the reactions that produce N, O, and  $N_4^+$  [*Sentman et al.*, 2008, and references therein]. The radiative lifetime of  $a^1\Sigma_u^- - X^1\Sigma_g^+$  is 0.5 s, since its Einstein coefficient is  $2 \text{ s}^{-1}$ . Comparing with Einstein coefficients of other  $N_2$  emission bands (Table 1), the Einstein coefficient of the radiative transition  $a^1\Sigma_u^- - X^1\Sigma_g^+$  is smaller. The radiative transfer calculations of this transition is relatively weak. Besides, the 108–200 nm emissions in the Ogawa-Tanaka-Wilkinson-Mulliken band system [*Lofthus and Krupenie*, 1977] is not considered of interest in the study of 762 nm emissions of sprites.

[34] The quenching processes with  $O_2$  and  $N_2$  are  $N_2(a^1\Sigma_u^-) + O_2 \rightarrow N_2(B^3\Pi_g) + O_2$  and  $N_2(a^1\Sigma_u^-) + N_2 \rightarrow N_2(B^3\Pi_g) + N_2$ . The quenching reaction rate constant is four orders of magnitude higher for  $O_2$  than that for  $N_2$  [*Kamaratos*, 2009, and references therein]. The fractional reduction rate  $\left(\frac{d[N_2(a^1\Sigma_u^-)]/dt}{[N_2(a^1\Sigma_u^-)]}\right)$  of  $N_2(a^1\Sigma_u^-)$  through the quenching reaction with  $O_2$  is the  $O_2$  density ( $3 \times 10^{14} \text{ cm}^{-3}$ ) times the reaction rate constant ( $3.2 \times 10^{-11} \text{ cm}^3 \text{ s}^{-1}$ ) =  $10^4 \text{ s}^{-1}$ . The time for the density of  $N_2(a^1\Sigma_u^-)$  to drop from  $10^5 \text{ cm}^{-3}$  to  $1 \text{ cm}^{-3}$  is  $-\ln(10^{-5}) \times 0.1 \text{ ms} \sim 1 \text{ ms}$ . The substate  $N_2(B^3\Pi_g)$  has a maximum density of  $10^5 \text{ molecules cm}^{-3}$ . Hence, the photon emission rate is

estimated to have a maximum value of  $10^5 \text{ cm}^{-3} \times 1.7 \times 10^4 \text{ s}^{-1} \sim 10^9 \text{ photons cm}^{-3} \text{ s}^{-1}$ .

[35] With the inclusion of these new vibrational kinetics (section 4.1), the density of  $N_2(X, v \leq 4)$  and  $N_2(X, v > 4)$  are computed to be increased to  $2.3 \times 10^9$  and  $1.2 \times 10^8 \text{ molecules cm}^{-3}$ , respectively, in  $\sim 10 \mu\text{s}$ , under the driving of a transient electric pulse that is  $5 E_k$  at the streamer tip and  $0.5 E_k$  in the streamer body during a  $\sim 1 \text{ ms}$  interval. The  $N_2$  density is  $\sim 1.2 \times 10^{15} \text{ molecules cm}^{-3}$  at the altitude of 70 km. The ratio of  $N_2(X, v > 4)$  to  $N_2$  is only  $10^{-7}$ , two orders of magnitude lower than the assumed  $10^{-5}$  by *Kamaratos* [2009]. Hence, the production rate of  $N_2(B^3\Pi_g)$  in the 1 ms E field driving period is expected to be weaker than that by *Kamaratos* [2009]. The density of  $N_2(A^3\Sigma_u^+)$  is up to  $1.4 \times 10^7 \text{ molecules cm}^{-3}$ , and rate of the chemical reaction in equation (4) is  $6.7 \times 10^4 \text{ molecules cm}^{-3} \text{ s}^{-1}$  ( $4.0 \times 10^{-11} \text{ cm}^3 \text{ molecules}^{-1} \text{ s}^{-1} \times 1.4 \times 10^7 \text{ molecules cm}^{-3} \times 1.2 \times 10^8 \text{ molecules cm}^{-3}$ ). That is also two orders of magnitude lower than the expected reaction rate for the production of  $N_2(B^3\Pi_g)$  in reaction (4). The change rate of  $N_2(B^3\Pi_g)$ ,  $d[N_2(B^3\Pi_g)]/dt$ , is  $[N_2(A^3\Sigma_u^+)] \times [N_2(X, v > 4)] \times \text{reaction rate} = 1.4 \times 10^7 \text{ molecules cm}^{-3} \times 1.2 \times 10^8 \text{ molecules cm}^{-3} \times 4 \times 10^{-11} \text{ cm}^3 \text{ molecules}^{-1} \text{ s}^{-1} = 10^5 \text{ molecules cm}^{-3} \text{ s}^{-1}$ . Therefore, 1 ms after switching off the electric field, the density of  $N_2(B^3\Pi_g)$  drops down to  $10^5 \text{ molecules cm}^{-3} \times 10^{-3} \text{ s} \sim 100 \text{ molecules cm}^{-3}$ . The photon emission rate is thereby reduced from the maximum value to  $10^2 \text{ molecules cm}^{-3} \times 1.7 \times 10^4 \text{ s}^{-1} \sim 10^6 \text{ photons cm}^{-3} \text{ s}^{-1}$ .

[36] To track the temporal evolution of the  $N_2(B^3\Pi_g)$  density after switching off the driving E field, four types of reactions are considered, and the production and the loss rates of  $N_2(B^3\Pi_g)$  via aforementioned reactions: (1) the cascading  $2PN_2$  radiative reaction, R105 (50 ns lifetime), (2) the quench crossing processes of  $N_2(a^1\Sigma_u^-)$  with  $O_2$  and  $N_2$  ( $\sim 1 \text{ ms}$  persisting duration), R100 and E5\*, where reaction E5\* indicates  $N_2(a^1\Sigma_u^-) + N_2 \rightarrow N_2(B^3\Pi_g) + N_2$ , listed before, (3) chemical excitation occurring by way of the energy pooling of  $N_2(A^3\Sigma_u^+)$  or  $O_2(a^1\Delta_g)$ , R91 and R90, and (4) the  $N_2$  vibrational kinetics that can last for several milliseconds, E4\*, are shown in Figure 7.

[37] In Figure 3, the density profile of  $N_2(a^1\Sigma_u^-)$  denoted by the black curve is tightly correlated with that of  $N_2(B^3\Pi_g)$ . This reflects the fact that the quenching cross process of  $N_2(a^1\Sigma_u^-)$  leading to increase of in  $N_2(B^3\Pi_g)$  is effective for a period of  $\sim 1$ – $2 \text{ ms}$ . Comparing with the other processes, the vibrational excitation of  $N_2(B^3\Pi_g)$ ,  $N_2(A) + N_2(X, v = 5 - 9) \rightarrow N_2(B) + N_2(X, v' < v)$ , can persist for several minutes because of the long vibrational relaxation time of  $5$ – $7 \text{ min}$  [*Picard et al.*, 1997]. Hence after switching off the E field, the production of  $N_2(B^3\Pi_g)$  is mainly sustained by  $N_2(X, v = 5 - 9)$ .

[38] As shown in Figure 7a, after about a couple of milliseconds from switching off the electric field (at 1 ms), the dominant  $N_2(B^3\Pi_g)$  producing reactions in the afterglow region are the reactions R90 (green dotted lines) and E4\* (green dashed lines). Comparing with the reaction R91,  $N_2(A) + N_2(A) \rightarrow N_2(B) + N_2(X, v' < v)$ , the reaction R90  $N_2(A) + O_2(a) \rightarrow N_2(B) + O_2$ , is expected to have a higher reaction rate than that of the R91 after switching off the E field; Figure 7a. The number density of  $O_2(a^1\Delta_g)$  is expected to decrease slower than that for  $N_2(A^3\Sigma_u^+)$ , shown in Figure 3,

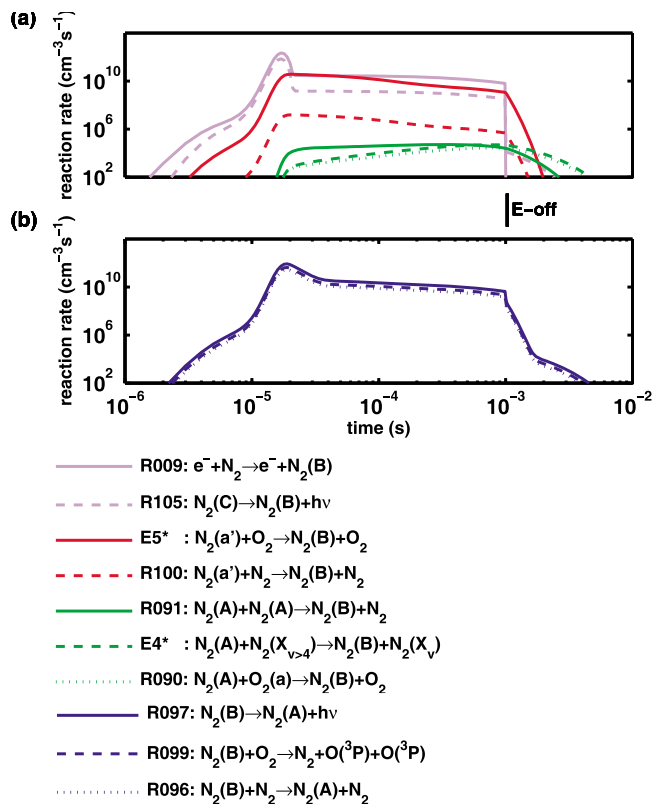


**Figure 7.** The chemical reaction rates for the production of the  $1PN_2$  band emissions,  $N_2(B^3\Pi_g) \rightarrow N_2(A^3\Sigma_u^+)$ : (a) the chemical reaction rate to populate the  $N_2(B^3\Pi_g)$  upper state and (b) the chemical reaction rate for the loss of the  $N_2(B^3\Pi_g)$  upper state.

because  $O_2(a^1\Delta_g)$  has a longer lifetime than that of  $N_2(A^3\Sigma_u^+)$ . The quenching rate for  $O_2(a^1\Delta_g)$  with  $N_2$  and  $O_2$  is also lower than that of  $N_2(A^3\Sigma_u^+)$ .

[39] Arguably in the 762 nm passband, the long persisting emissions ( $>30$  ms) at the sprite altitudes may not exclusively come from  $O_2$  atm (0, 0) emissions. It could also come from dancing sprites or streamer beads. The emissions due to continuing currents at the cloud deck level [Cummer *et al.*, 2006] can also be the source of the long 762 nm emissions. However, the cloud level emissions are well separated from the sprite altitudes in the limb-viewing ISUAL imager (Figure 6a), thus the persisting 762 nm emissions in the upper region of the images clearly are not cloud emissions. Furthermore, all the four 762 nm sprites studied here are not dancing sprites and contained no recognizable bead structures. From our experience, the sensitivity of the ISUAL imager is high enough to detect the bead structures as well as their emissions. Hence the detected persisting 762 nm emissions are most likely coming from the  $O_2$  atm (0, 0) bands.

[40] Due to the strong absorption of the 762 nm emissions by  $O_2$  below 60 km, the sprite emissions in this band were much reduced in the sprite spectra measured from the ground [Mende *et al.*, 1995; Green *et al.*, 1996; Hampton *et al.*, 1996; Kanmae *et al.*, 2007, 2010]. However, in the ISUAL 762 nm sprites, in addition to the sprite emissions, the imager frames in Figures 6a–6e contain much stronger emissions from the parent lightning in this band. For the current and upcoming

TLE-detection satellite missions, the intensity ratio of lightning emissions to sprite emissions (L/S) would be a key measurement for identifying the relative weak sprite signals embedded in the strong emissions of lightning, especially for nadir spacecraft observations. The four 762 nm sprites analyzed here were recorded by ISUAL in a limb-viewing configuration. Under the exposure time of 30 ms, the average 762 nm brightness in the first imager frame are  $\sim 200$ ,  $\sim 120$ , 320 and 180 kR for the four sprites, respectively, while it is 250, 230, 180 and 210 kR for their parent lightning. The L/S ratios are 1.3, 1.9, 0.6, and 1.2. If the maximum brightness of sprites and parent lightning are used, then the L/S ratios have even higher values of 2.5, 11.7, 0.6 and 3.5, respectively. Hence for spacecraft nadir TLE-detection missions, 762 nm band may not be a reliable signature for distinguishing sprite events, and thus auxiliary emission bands are needed.

## 6. Summary

[41] To understand the origin of these emissions, a zero-dimensional plasma chemistry model was employed to compute the luminous duration and the brightness of the major sprite emissions in the ISUAL imager 762 nm passband. For a sprite streamer at 70 km, if the pulse electric field is  $5 E_k$  in the streamer head (6  $\mu$ s) and  $0.5 E_k$  in the streamer body (1 ms), the model indicates the first positive bands of molecular nitrogen ( $1PN_2$ ), the atmospheric bands of molecular oxygen ( $O_2$  atm), and the hydroxyl (OH) emissions are the major sprite emissions in this passband. The theoretical brightness of the  $1PN_2$ ,  $O_2$  atm, and OH emissions in a single streamer is 1.4 MR, 2.6 kR, and 1.3 R, respectively, averaging over 30 ms. After converting and factoring in the 762 nm filter transmittance of the  $1PN_2$ ,  $O_2$  atm, and OH band emissions, the predicted brightness of these bands in the long-duration sprite is 1 MR, 30 kR, and  $\sim 0$ , respectively. The model further indicates that in the 762 nm passband only the  $O_2$  atm emissions will persist for 1 s, after the sprite initiation. With the luminous duration and the brightness consistent or close to that predicted, it is therefore concluded that the long persisting emissions detected in the 762 nm sprites was from the  $O_2$  atm (0, 0) bands.

[42] In the ISUAL 762 nm sprite campaign, bright 762 nm lightning emissions were also detected; even though they are expected to be severely absorbed by molecular oxygen in the lower atmosphere. Through the 762 nm narrow band filter, the parent lightning was found to be nearly twice as bright as the sprite. Hence for spacecraft nadir TLE-detection missions, 762 nm bands may not be used as the sole signature in differentiating sprite events and additional auxiliary emission bands needed to be explored.

[43] **Acknowledgments.** Works were supported in part by the National Space Organization (NSPO) and the National Science Council (NSC) in Taiwan under grants 98-NSPO(B)-ISUAL-FA09-01, NSC96-2112-M-006-003-MY3, NSC97-2111-M-006-001-MY3, NSC97-2111-M-006-004-MY3, and NSC98-2111-M-008-001. T.-Y. Huang acknowledges support from the U.S. NSF grant AGS-0836920 to Pennsylvania State University and the Taiwan's National Science Council (NSC) grant NSC 98-2811-M-006-018 to National Cheng Kung University. We are grateful to the National Center for High-Performance Computing for computer time and facilities.

[44] Robert Lysak thanks Efstathios Kamaratos and another reviewer for their assistance in evaluating this paper.

## References

- Babcock, H. D., and L. Herzberg (1948), Fine structure of the red system of atmospheric oxygen bands, *Astrophys. J.*, *108*, 167–190, doi:10.1086/145062.
- Belyaev, A. N., V. V. Alpatov, E. Blanc, and V. E. Melnikov (2006), Space-based observations of O<sub>2</sub> A (0, 0) band emission near the solar terminator and their interpretation, *Adv. Space Res.*, *38*, 2366–2373, doi:10.1016/j.asr.2006.05.021.
- Blanc, E., and F. Lefeuvre (2006), TARANIS: A microsatellite project dedicated to the study of impulsive transfers of energy between the Earth atmosphere-ionosphere and magnetosphere, paper presented at 36th COSPAR Scientific Assembly, Comm. on Space Res., Beijing.
- Brasseur, G., and S. Solomon (1986), *Aeronomy of the Middle Atmosphere: Chemistry and Physics of the Stratosphere and Mesosphere*, 2nd rev. ed., 441 pp., D. Reidel, Dordrecht, Netherlands.
- Chang, S. C., et al. (2010), ISUAL far-ultraviolet events, elves, and lightning current, *J. Geophys. Res.*, *115*, A00E46, doi:10.1029/2009JA014861.
- Chen, B., et al. (2008), Global distributions and occurrence rates of transient luminous events, *J. Geophys. Res.*, *113*, A08306, doi:10.1029/2008JA013101.
- Chern, J. L., R. R. Hsu, H. T. Su, S. B. Mende, H. Fukunishi, Y. Takahashi, and L. C. Lee (2003), Global survey of upper atmospheric transient luminous events on the ROCSAT-2 satellite, *J. Atmos. Terr. Phys.*, *65*, 647–659, doi:10.1016/S1364-6826(02)00317-6.
- Chou, J. K., et al. (2010), Gigantic jets with negative and positive polarity streamers, *J. Geophys. Res.*, *115*, A00E45, doi:10.1029/2009JA014831.
- Cummer, S. A., H. U. Frey, S. B. Mende, R. Hsu, H. Su, A. B. Chen, H. Fukunishi, and Y. Takahashi (2006), Simultaneous radio and satellite optical measurements of high-altitude sprite current and lightning continuing current, *J. Geophys. Res.*, *111*, A10315, doi:10.1029/2006JA011809.
- Gerken, E. A., and U. S. Inan (2003), Observations of decameter-scale morphologies in sprites, *J. Atmos. Terr. Phys.*, *65*, 567–572, doi:10.1016/S1364-6826(02)00333-4.
- Gerken, E. A., U. S. Inan, and C. P. Barrington-Leigh (2000), Telescopic imaging of sprites, *Geophys. Res. Lett.*, *27*, 2637–2640, doi:10.1029/2000GL000035.
- Gilmore, F. R., R. R. Laher, and P. J. Espy (1992), Franck-Condon factors, r-centroids, electronic transition moments, and Einstein coefficients for many nitrogen and oxygen band systems, *J. Phys. Chem. Ref. Data*, *21*, 1005–1107, doi:10.1063/1.555910.
- Goldman, A., W. G. Schoenfeld, D. Goorvitch, C. Chackerian Jr., H. Dothe, F. Mélen, M. C. Abrams, and J. E. A. Selby (1998), Updated line parameters for OH X<sub>2</sub>II-X<sub>2</sub>II ( $\nu''$ ,  $\nu'$ ) transitions, *J. Quant. Spectrosc. Radiat. Transfer*, *59*, 453–469, doi:10.1016/S0022-4073(97)00112-X.
- Green, B. D., M. E. Fraser, W. T. Rawlins, L. Jeong, W. A. M. Blumberg, S. B. Mende, G. R. Swenson, D. L. Hampton, E. M. Wescott, and D. D. Sentman (1996), Molecular excitation in sprites, *Geophys. Res. Lett.*, *23*, 2161–2164, doi:10.1029/96GL02071.
- Greenblatt, G. D., J. J. Orlando, J. B. Burkholder, and A. R. Ravishankara (1990), Absorption measurements of oxygen between 330 and 1140 nm, *J. Geophys. Res.*, *95*, 18,577–18,582, doi:10.1029/JD095iD11p18577.
- Hampton, D. L., M. J. Heavner, E. M. Wescott, and D. D. Sentman (1996), Optical spectral characteristics of sprites, *Geophys. Res. Lett.*, *23*, 89–92, doi:10.1029/95GL03587.
- Hedin, A. E. (1991), Extension of the MSIS thermosphere model into the middle and lower atmosphere, *J. Geophys. Res.*, *96*, 1159–1172, doi:10.1029/90JA02125.
- Herman, R. C., and G. A. Hornbeck (1953), Vibration-rotation bands of OH, *Astrophys. J.*, *118*, 214–227, doi:10.1086/145744.
- Jursa, A. S. (1985), *Handbook of Geophysics and the Space Environment*, 4th ed., Air Force Geophys. Lab., Hanscom Air Force Base, Mass.
- Kamaratos, E. (2009), Comment on “Plasma chemistry of sprite streamers” by D. D. Sentman, H. C. Stenbaek-Nielsen, M. G. McHarg, and J. S. Morrill, *J. Geophys. Res.*, *114*, D08109, doi:10.1029/2008JD011196.
- Kanmae, T., H. C. Stenbaek-Nielsen, and M. G. McHarg (2007), Altitude resolved sprite spectra with 3 ms temporal resolution, *Geophys. Res. Lett.*, *34*, L07810, doi:10.1029/2006GL028608.
- Kanmae, T., H. C. Stenbaek-Nielsen, M. G. McHarg, and R. K. Haaland (2010), Observation of sprite streamer head’s spectra at 10,000 fps, *J. Geophys. Res.*, *115*, A00E48, doi:10.1029/2009JA014546.
- Khomich, V. Y., A. I. Semenov, and N. N. Shefov (2008), *Airglow as an Indicator of Upper Atmospheric Structure and Dynamics*, Springer, Berlin.
- Kosy, I., A. Kostinsky, A. Matveyev, and V. Siulakov (1992), Kinetic scheme of the non-equilibrium discharge in nitrogen-oxygen mixtures, *Plasma Sources Sci. Technol.*, *1*, 207–220, doi:10.1088/0963-0252/1/3/011.
- Kuo, C.-L., R. R. Hsu, A. B. Chen, H. T. Su, L. C. Lee, S. B. Mende, H. U. Frey, H. Fukunishi, and Y. Takahashi (2005), Electric fields and electron energies inferred from the ISUAL recorded sprites, *Geophys. Res. Lett.*, *32*, L19103, doi:10.1029/2005GL023389.
- Kuo, C. L., A. B. Chen, J. K. Chou, L. Y. Tsai, R. R. Hsu, H. T. Su, H. U. Frey, S. B. Mende, Y. Takahashi, and L. C. Lee (2008), Radiative emission and energy deposition in transient luminous events, *J. Phys. D: Appl. Phys.*, *41*, 234014, doi:10.1088/0022-3727/41/23/234014.
- Laux, C. O. (1993), Optical diagnostics and radiative emission of air plasmas, Ph.D. thesis, Stanford Univ., Stanford, Calif.
- Lee, L. J., et al. (2010), Controlling synoptic-scale factors for the distribution of the transient luminous events, *J. Geophys. Res.*, *115*, A00E54, doi:10.1029/2009JA014823.
- Li, J., and S. A. Cummer (2009), Measurement of sprite streamer acceleration and deceleration, *Geophys. Res. Lett.*, *36*, L10812, doi:10.1029/2009GL037581.
- Liu, N., and V. P. Pasko (2004), Effects of photoionization on propagation and branching of positive and negative streamers in sprites, *J. Geophys. Res.*, *109*, A04301, doi:10.1029/2003JA010064.
- Liu, N., and V. P. Pasko (2005), Molecular nitrogen LBH band system far-UV emissions of sprite streamers, *Geophys. Res. Lett.*, *32*, L05104, doi:10.1029/2004GL022001.
- Liu, N., et al. (2006), Comparison of results from sprite streamer modeling with spectrophotometric measurements by ISUAL instrument on FORMOSAT-2 satellite, *Geophys. Res. Lett.*, *33*, L01101, doi:10.1029/2005GL024243.
- Liu, N. Y., V. P. Pasko, K. Adams, H. C. Stenbaek-Nielsen, and M. G. McHarg (2009a), Comparison of acceleration, expansion, and brightness of sprite streamers obtained from modeling and high-speed video observations, *J. Geophys. Res.*, *114*, A00E03, doi:10.1029/2008JA013720.
- Liu, N., V. P. Pasko, H. U. Frey, S. B. Mende, H.-T. Su, A. B. Chen, R.-R. Hsu, and L.-C. Lee (2009b), Assessment of sprite initiating electric fields and quenching altitude of a <sup>1</sup>Π<sub>g</sub> state of N<sub>2</sub> using sprite streamer modeling and ISUAL spectrophotometric measurements, *J. Geophys. Res.*, *114*, A00E02, doi:10.1029/2008JA013735.
- Lofthus, A., and P. H. Krupenie (1977), The spectrum of molecular nitrogen, *J. Phys. Chem. Ref. Data*, *6*, 113–307, doi:10.1063/1.555546.
- Marsh, D. R., W. R. Skinner, A. R. Marshall, P. B. Hays, D. A. Ortlund, and J.-H. Yee (2002), High Resolution Doppler Imager observations of ozone in the mesosphere and lower thermosphere, *J. Geophys. Res.*, *107*(D19), 4390, doi:10.1029/2001JD001505.
- McDade, I. C., D. P. Murtagh, R. G. H. Greer, P. H. G. Dickinson, G. Witt, J. Stegman, E. J. Llewellyn, L. Thomas, and D. B. Jenkins (1986), ETON 2: Quenching parameters for the proposed precursors of O<sub>2</sub>(b<sup>1</sup>Σ<sub>g</sub><sup>+</sup>) and O(<sup>1</sup>S) in the terrestrial nightglow, *Planet. Space Sci.*, *34*(9), 789–800, doi:10.1016/0032-0633(86)90075-9.
- McHarg, M. G., H. C. Stenbaek-Nielsen, and T. Kammer (2007), Observations of streamer formation in sprites, *Geophys. Res. Lett.*, *34*, L06804, doi:10.1029/2006GL027854.
- Meinel, I. A. B. (1950), OH emission bands in the spectrum of the night sky, *Astrophys. J.*, *111*, 555, doi:10.1086/145296.
- Mende, S. B., R. L. Rairden, G. R. Swenson, and W. A. Lyons (1995), Sprite spectra; N<sub>2</sub> 1 PG band identification, *Geophys. Res. Lett.*, *22*, 2633–2636, doi:10.1029/95GL02827.
- Mende, S. B., H. U. Frey, R. R. Hsu, H. T. Su, A. B. Chen, L. C. Lee, D. D. Sentman, Y. Takahashi, and H. Fukunishi (2005), D region ionization by lightning-induced electromagnetic pulses, *J. Geophys. Res.*, *110*, A11312, doi:10.1029/2005JA011064.
- Pancheshnyi, S. V., S. M. Starikovskaya, and A. Y. Starikovskii (1997), Measurements of the rates of quenching of N<sub>2</sub> (C<sup>3</sup>Π<sub>u</sub>) and N<sub>2</sub><sup>+</sup> (B<sup>2</sup>Σ<sub>u</sub><sup>+</sup>) states by N<sub>2</sub>, O<sub>2</sub>, and CO molecules in the afterglow plasma of a nanosecond discharge, *Plasma Phys. Rep.*, *23*, 616–620.
- Pasko, V. P., U. S. Inan, and T. F. Bell (1998), Spatial structure of sprites, *Geophys. Res. Lett.*, *25*, 2123–2126, doi:10.1029/98GL01242.
- Picard, R. H., U. S. Inan, V. P. Pasko, J. R. Winick, and P. P. Wintersteiner (1997), Infrared glow above thunderstorms?, *Geophys. Res. Lett.*, *24*, 2635–2638, doi:10.1029/97GL02753.
- Piper, L. G. (1992), Energy transfer studies on N<sub>2</sub> (X<sup>1</sup>Σ<sub>g</sub><sup>+</sup>, v) and N<sub>2</sub> (B<sup>3</sup>Π<sub>g</sub>), *J. Chem. Phys.*, *97*, 270–275, doi:10.1063/1.463625.
- Piper, L. G. (1994), Further observations on the nitrogen orange afterglow, *J. Chem. Phys.*, *101*, 10,229–10,236, doi:10.1063/1.467903.
- Sander, S. P., et al. (2003), Chemical kinetics and photochemical data for use in atmospheric studies, *Evaluation No. 14, JPL Publication 02–25*, Jet Propul. Lab., Pasadena, Calif.
- Sentman, D. D., and H. C. Stenbaek-Nielsen (2009), Chemical effects of weak electric fields in the trailing columns of sprite streamers, *Plasma*

- Sources Sci. Technol.*, 18(3), 034012, doi:10.1088/0963-0252/18/3/034012.
- Sentman, D. D., E. M. Wescott, D. L. Osborne, D. L. Hampton, and M. J. Heavner (1995), Preliminary results from the Sprites94 aircraft campaign: 1. Red sprites, *Geophys. Res. Lett.*, 22, 1205–1208, doi:10.1029/95GL00583.
- Sentman, D. D., H. C. Stenbaek-Nielsen, M. G. McHarg, and J. S. Morrill (2008), Plasma chemistry of sprite streamers, *J. Geophys. Res.*, 113, D11112, doi:10.1029/2007JD008941.
- Slanger, T. G., and R. A. Copeland (2003), Energetic oxygen in the upper atmosphere and the laboratory, *Chem. Rev.*, 103, 4731–4766, doi:10.1021/cr0205311.
- Stenbaek-Nielsen, H. C., and M. G. McHarg (2008), High time-resolution sprite imaging: Observations and implications, *J. Phys. D: Appl. Phys.*, 41, 234009, doi:10.1088/0022-3727/41/23/234009.
- Stenbaek-Nielsen, H. C., M. G. McHarg, T. Kanmae, and D. D. Sentman (2007), Observed emission rates in sprite streamer heads, *Geophys. Res. Lett.*, 34, L11105, doi:10.1029/2007GL029881.
- Takahashi, Y., K. Yoshida, Y. Sakamoto, and T. Sakamoi (2010), SPRITE-SAT: A university small satellite for observation of high-altitude luminous events, in *Small Satellite Missions for Earth Observation*, edited by R. Sandau, H.-P. Roser, and A. Valenzuela, pp. 197–206, Springer, Berlin.
- Umemoto, H., M. Oku, and T. Iwai (2003), Collisional intersystem crossing of  $N_2(a^1\Sigma_u^-)$  to produce triplet-state molecular nitrogen, *J. Chem. Phys.*, 118(22), 10,006–10,011, doi:10.1063/1.1573188.
- Vallance-Jones, A. (1974), *Aurora*, D. Reidel, Dordrecht, Netherlands.
- Van Zyl, B., and W. Pendleton (1995),  $N_2^+(X)$ ,  $N_2^+(A)$ , and  $N_2^+(B)$  production in  $e^-+N_2$  collisions, *J. Geophys. Res.*, 100, 23,755–23,762, doi:10.1029/95JA02699.
- 
- S. C. Chang, R. R. Hsu, T. Y. Huang, C. L. Kuo, L. J. Lee, and H. T. Su, Department of Physics, National Cheng Kung University, No. 1, Ta-Hsueh Rd., Tainan, 70101 Taiwan. (johnny@phys.ncku.edu.tw)
- A. B. Chen, Institute of Space, Astrophysical and Plasma Sciences, National Cheng Kung University, 1 University Rd., Tainan, 70101 Taiwan.
- H. U. Frey and S. B. Mende, Space Sciences Laboratory, University of California, 7 Gauss Way, Berkeley, CA 94720, USA.
- L. C. Lee, Institute of Space Science, National Central University, 300 Jhongda Rd., Jhongli, 32001 Taiwan.
- D. D. Sentman, Geophysical Institute, University of Alaska Fairbanks, PO Box 757320, Fairbanks, AK 99775, USA.
- Y. Takahashi, Department of CosmoSciences, Hokkaido University, 8-2-08, Kita-10, Nishi-8, Kita-ku, Sapporo, 060-0810 Japan.